Journal of Alloys and Compounds 619 (2015) 616–620

Contents lists available at ScienceDirect

Journal of Alloys and Compounds

journal homepage: www.elsevier.com/locate/jalcom

Effect of B and Cr on elastic strength and crystal structure of Ni_3Al alloys under high pressure

S.V. Raju [a,*], A.A. Oni [b], B.K. Godwal [c], J. Yan [d,e], V. Drozd [a], S. Srinivasan [f], J.M. LeBeau [b], K. Rajan [f], S.K. Saxena [a]

[a] CeSMEC, Dept. of Mechanical Engr., Florida International University, Miami, FL 33172, USA
[b] Department of Materials Science and Engr., North Carolina State University, Raleigh, NC 27695, USA
[c] Department of Earth and Planetary Sciences, University of California, Berkeley, CA 94720, USA
[d] Advanced Light Source, Lawrence Berkeley National Laboratory, Berkeley, CA 94730, USA
[e] Earth & Planetary Sciences Department, University of California, Santa Cruz, CA 95064, USA
[f] Department of Materials Science and Engg., Iowa State University, Iowa, IA, USA

ARTICLE INFO

Article history:
Received 27 May 2014
Received in revised form 29 August 2014
Accepted 1 September 2014
Available online 16 September 2014

Keywords:
Superalloys
High pressure
X-ray diffraction
Nano-indentation
Elastic properties

ABSTRACT

Samples of Ni_3Al, Ni_3Al:B and Ni–Al–Cr super alloys were prepared by directional solidification method and their effect of alloying with ternary elements on the mechanical properties was investigated. In-situ X-ray diffraction studies were carried out on undoped Ni_3Al, Ni_3Al:B with boron 500 ppm and Ni–Al–Cr with 7.5 at.% of chromium super alloys at high pressure using diamond anvil cell. The results indicate that micro-alloying with B forms γ′-phase ($L1_2$ structure), similar to the pure Ni $_3$Al, while Ni–Al–Cr alloy consists of γ′ precipitates in a matrix of γ-phase (Ni-FCC structure). The crystal structure of all three alloys was stable up to 20 GPa. Micro alloying with boron increases bulk modulus of Ni_3Al by 8% whereas alloying with chromium has the opposite effect decreasing the modulus by 11% when compared to undoped alloy. Further, the elastic modulus and hardness of Ni_3Al, Ni_3Al:B and Ni–Al–Cr alloys were determined using the nano-indentation technique, in combination with compressibility data which enabled the estimation of shear modulus and Poisson's ratio of these alloys.

1. Introduction

Ni_3Al has received much attention as a high temperature structural material for applications in aerospace due to its low density, high melting point and excellent oxidation resistance property [1–5]. However, its intrinsic brittleness and poor tolerance to damage at room temperature and low creep strength at elevated temperatures have heavily retard its usefulness to actual application. To overcome these challenges, commercial superalloys are typically alloyed with Ni, Fe, Cr and Co as the major elements. Several other trace elements are also added towards increasing the defects and dislocations in order to increase their mechanical strength without altering the crystal structure. The combination of Cr and B, for example, leads to simultaneously improved corrosion resistance, yield strength and ductility [6].

Ni_3Al has highly ordered $L1_2$-type cubic structure with space group $Pm\bar{3}m$ and are known to be the hardest phase in the Ni–Al system [5,6]. Alloying Ni_3Al with chromium reduces the amount of aluminum required to form Al_2O_3 which acts as protective coating in oxidizing and corrosive environments [7,8]. Addition of Cr forms a two-phase composite system consisting of γ and γ′ phases [6]. We know that Cr preferentially partitions to the γ phase because the atomic radius is very similar to that of Ni [9]. A number of studies have investigated the partitioning of transition metal elements (such as Cr, Co, W, and Ta) using both experimental and computational methods. Further, previous atom-probe tomography (APT), scanning electron microscopy (SEM), and atom location by channeling enhanced microanalysis (ALCHEMI) technique have concluded that Cr occupies the Al sub lattice in the γ′ phase [10–12]. Chowdry et al. [12] studied the site occupancy behavior of Cr in γ′-Ni_3Al using *ab initio* Density Functional Theory (DFT) computational studies and 3D atom probe tomography (APT). Their results show that chromium atoms prefer to be close by on either nickel or aluminum sublattices or on a nickel–aluminum mixed lattice, suggesting a potential tendency of chromium segregation in the γ′ phase. In our work, Ni–Al–Cr with nominal composition 75.7Ni–16.7Al–7.6Cr at.% was chosen such that both the γ

* Corresponding author.
E-mail address: sraju@fiu.edu (S.V. Raju).

http://dx.doi.org/10.1016/j.jallcom.2014.09.012
0925-8388/

and γ′ phases are stable [13]. Micro alloying of boron with Ni_3Al is known to improve the mechanical properties by suppressing embrittlement and strengthening grain boundaries [14–16]. Muller et al. [17] studied the role of boron in ductilizing grain boundaries from structural, chemistry and bonding aspects. From micro hardness studies, Qian and Chou [18] reported that for alloys near-stoichiometric composition, the maximum ductilizing effect occurred at about 500 ppm (0.23 at.%) boron. Further, they proposed a cross slip of screw dislocations as the reason for the ductilizing effect. Hence, we have chosen Ni_3Al:B with nominal composition 75Ni–25Al + 500 pm–B.

Several authors in the past few decades have studied the effect of alloying on the bulk mechanical properties most commonly by SEM and other bulk ex-situ measurements [19]. Furthermore, considerable theoretical work has been completed in an attempt to further understand the dopants that are likely to enhance elastic properties beyond current state-of-the art materials [20]. Recent study using density functional (DFT) calculations on chemical pressure effect, for example, aim to identify those specific atoms in the crystal lattice that significantly contribute to the increase in the structural and elastic properties [21]. Pressure dependent studies of these system have, however, been lacking in the literature for comparison with theory efforts. In this study, we have chosen B and Cr in an effort to understand and correlate the effect of alloying with ternary elements on the elastic strength and crystal structure of Ni_3Al. We have carried out in-situ X-ray diffraction studies on alloys of Ni_3Al, Ni_3Al:B (500 ppm of B), Ni–Al–Cr (7.5 at.% of Cr) at high pressures using diamond anvil cell. Further, nano-indentation measurements were carried out to determine the elastic modulus and hardness.

2. Experimental

2.1. Sample preparation and X-ray diffraction

Elemental powders of Ni_3Al, Ni_3Al:B (500 ppm) and Ni–Al–Cr with (Cr 7.5 at.%) were mixed in stoichiometric ratio and made into pellets. Directionally solidified alloys were made by Bridgman–Stockburger technique, the details can be found elsewhere [22]. X-ray diffraction (XRD) pattern were collected on each of these alloys. Previous studies show that Boron segregates at the grain boundaries whereas Cr addition forms two phase system with γ and γ′ [23]. Hence, X-ray diffraction XRD data of Ni_3Al doped with boron of 500 ppm was fitted to $Pm\bar{3}m$ ($L1_2$ phase) while Ni–Al–Cr XRD data was fitted to $Pm\bar{3}m$ ($L1_2$) and Ni-type (FCC) phases. Lattice parameters obtained from the X-ray diffraction pattern are listed in Table 1 and the results are found to be in agreement with the literature [24,25]. The alloys were further characterized by electron microscopy techniques, further their elastic properties were measured using *in-situ* X-ray diffraction under high pressure and nano indentation measurements. The experimental details and results are presented in the section below.

2.2. Electron microscopy

TEM samples were prepared by conventional mechanical polishing followed by low-energy ion milling. A probe-corrected FEI Titan G2 60–300 kV S/TEM equipped with an X-FEG source and state-of-the-art Super-X EDS detector system was operated at 200 kV for HAADF-STEM imaging and EDS mapping. The convergence and inner collection semi-angles for the Titan S/TEM were 15 mrad and 77 mrad, respectively. High-annular angle dark field (HAADF) technique whereby the atom contrast is proportional to the atomic number Z of the scattering atoms was employed for STEM imaging. HAADF-STEM image series were acquired and post-processed using the RevSTEM technique to correct for the sample drift distortion and to significantly enhance the signal-to-noise ratio [26]. The EDS maps were formed using X-ray lines: Ni–K, Al–K and Cr–K.

Table 1
Crystal structure and lattice parameters of Ni–Al alloys studied.

Alloy	S.G	Lattice parameters	
		a (A)	v (A^3)
Ni_3Al	$Pm\bar{3}m$	3.572 ± 0.013	45.58
Ni_3Al:B (500 ppm)	$Pm\bar{3}m$	3.577 ± 0.005	45.80
Ni–Al–Cr (7.5 at.% Cr) 2-Phase	$Pm\bar{3}m$, $Fm\bar{3}m$	3.567 ± 0.005	45.38

2.3. In-situ X-ray diffraction using DAC

In-situ X-ray diffraction studies were carried out on Ni_3Al:B at B1 station, CHESS, Ithaca in angle dispersive geometry at a wavelength 0.4858 Å. Ni_3Al and Ni–Al–Cr were studied in angle dispersive geometry using wavelength 0.4959 Å at beamline 12.2.2, of Advanced Light Source (ALS), LBNL, Berkeley. The details of the experimental set-up at both facilities can be found elsewhere [27,28].

For XRD at high pressures, alloys were loaded in diamond anvil cell. A stainless steel gasket was indented to 50 μm thickness and a 200 μm hole was drilled which serves as the sample chamber. Pre-indented gasket was placed in between the culets of the two opposed diamond anvils. Methanol–ethanol mixture in the ratio of 4:1 was loaded along with the sample which served as pressure transmitting medium. Ni_3Al:B was investigated up to 25 GPa. The crystal structure at ambient conditions was found to have γ′ phase which remained stable up to 20 GPa, the highest pressure studied.

2.4. Nano-indentation

Nano-indentation tests were carried out using Hysitron Triboindenter (Hysitron, Minneapolis, USA) with a diamond Berkovich indenter tip of 100 nm tip radius. The details of the technique can be found elsewhere [29]. Nano indentation was performed at the loading rate of 25 μN/s up to a peak load of 1000 μN where it was held for 2 s and then unloaded completely at negative rate of 25 μN/s. The hardness and elastic modulus were calculated by the Oliver and Pharr method [30,31]. Samples were mounted on an epoxy mold and polished to mirror finish using Al_2O_3 particles of various sizes down to 0.3 μm. The sample was then placed in the Tribo-nanoindentor and applied load in the range 0–2000 μN.

3. Results and discussion

3.1. Crystal structure and elemental mapping

Pure Ni_3Al and B-doped Ni_3Al alloys formed only $L1_2$ structure at ambient conditions, whereas Ni–Al–Cr forms a two-phase composite system consisting of an ordered $L1_2$-type (γ′) phase and a disordered FCC (γ) phase. HAADF-STEM image of the Ni_3Al:B alloy along the ⟨100⟩ projection is presented in Fig. 1(a). Because of the low concentration and atomic number (Z = 5), the efficiency of the B X-ray signals is not sufficient enough to be detected in the EDS map. The presence of γ and γ′ phases are highlighted in the EDS elemental maps of the Ni–Al–Cr superalloy, shown in Fig. 1(b). The preferential partitioning of Cr, a well-known γ-stabilizing element, to the γ phase is consistent with predictions in literature [9,32]. Fig. 1(b) shows the HAADF-STEM image of a γ/γ′ interface in the Ni–Al–Cr superalloy. In the γ′ phase, Ni (Z = 28) and Al (Z = 13) occupy the high and low intensity atom columns, respectively, while those in the γ phase exhibit similar intensity. According to literature [10], we expect the Cr to preferentially occupy the Al sub-lattice in the ordered γ′ phase.

3.2. Bulk modulus using XRD under high pressure

Figs. 2–4 show the X-ray diffraction patterns collected in angle dispersive geometry for Ni_3Al, Ni_3Al:B and Ni–Al–Cr, respectively at various pressures under hydrostatic conditions. From the XRD data, pressure–volume data were extracted for all the three alloys. Fig. 5 shows the P–V equation of state fit, which was obtained using third order Birch–Murnaghan equation [34,35] of state given by,

$$P(V) = \frac{3B_0}{2}\left[\left(\frac{V_0}{V}\right)^{\frac{7}{3}} - \left(\frac{V_0}{V}\right)^{\frac{5}{3}}\right]\left\{1 + \frac{3}{4}(B_0' - 4)\left[\left(\frac{V_0}{V}\right)^{\frac{2}{3}} - 1\right]\right\} \quad (1)$$

From the fit, bulk modulus and its first order pressure derivative were determined. The results obtained are given in Table 2. Crystal structures of all three alloys studied are found to be stable up to 20 GPa, the highest pressure studied.

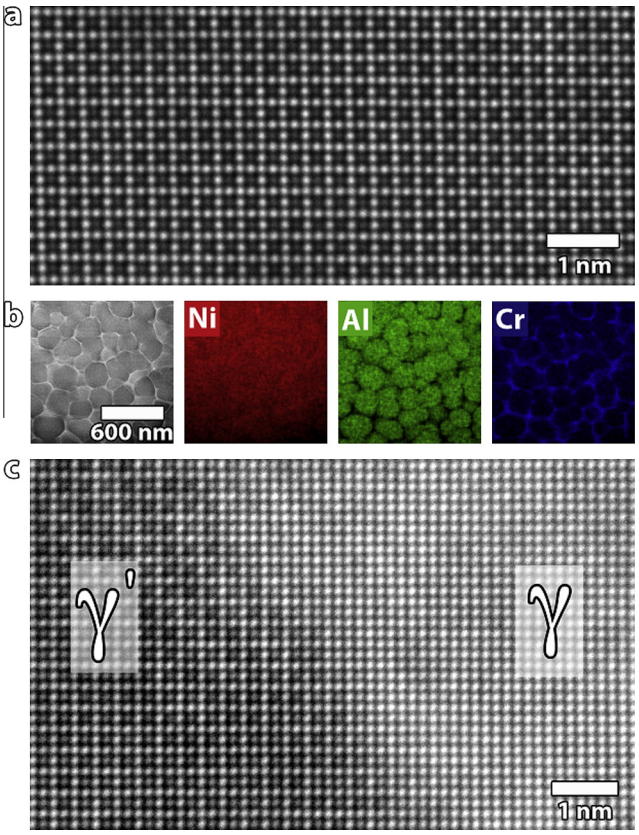

Fig. 1. (a) HAADF-STEM image of Ni_3Al:B superalloy along the ⟨100⟩ projection. (b) EDS elemental maps of the Ni–Al–Cr superalloy microstructure clearly showing the presence of γ and γ′ phases. (c) HAADF-STEM image of the coherent γ/γ′ interface in the Ni–Al–Cr superalloy.

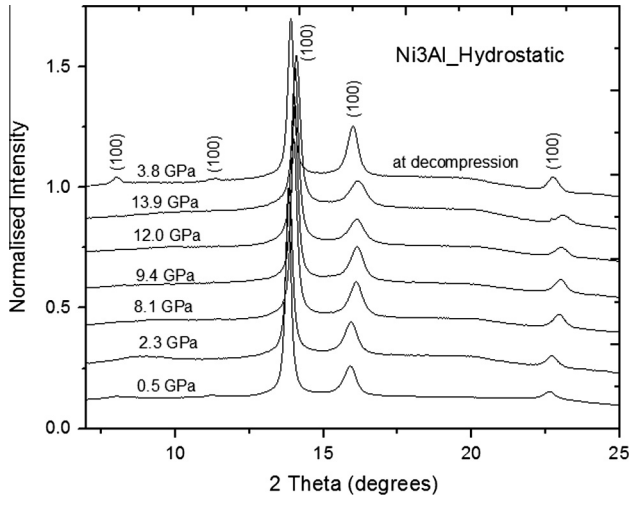

Fig. 2. X-ray diffraction pattern of Ni_3Al at various pressures. Ruby fluorescence line shift was used for pressure measurement.

3.3. Elastic modulus and hardness

Fig. 6 shows the loading and unloading curve obtained for the three alloys studied. The loading and unloading was repeated six times and the average of hardness and elastic modulus were obtained. It is well known that during nano indentation the maximum displacement (h_m) at the peak load equals the sum of the contact depth (h_c) and the elastic surface displacement at the perimeter of the contact (h_s) [42].

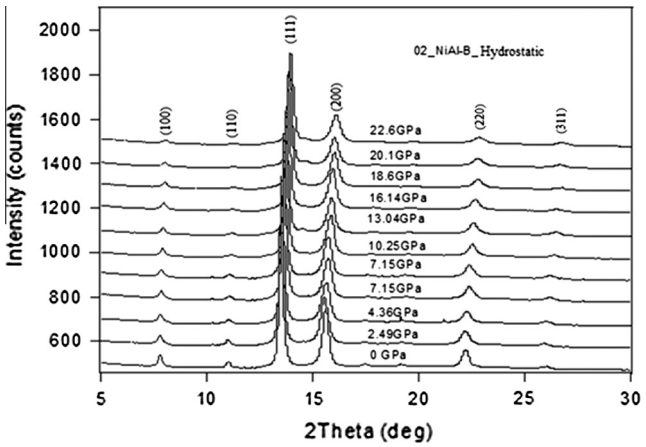

Fig. 3. X-ray diffraction pattern of Ni_3Al:B (500 ppm) at various pressures. Pressure was measured using fluorescence line shift of ruby.

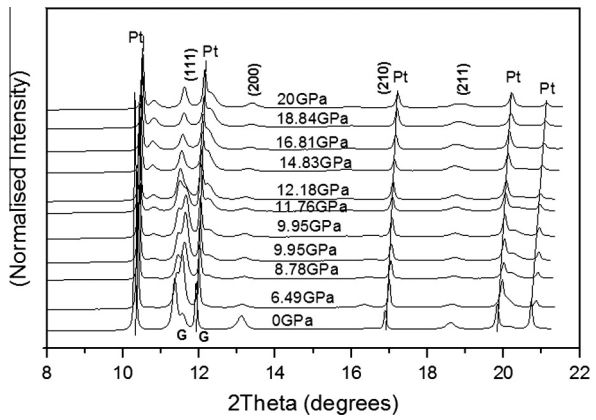

Fig. 4. X-ray diffraction pattern of Ni–Al–Cr (7.5 at.%) at various pressures. Pt refers to platinum peak positions from which the pressure at each step was determined using its equation of state [33].

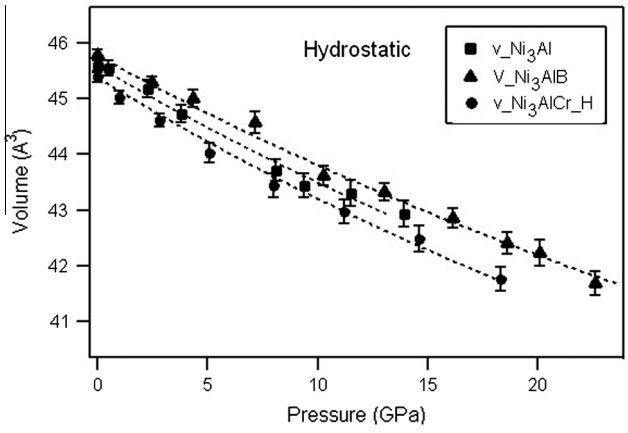

Fig. 5. Pressure *vs.* volume data obtained for line represents the third order Birch–Murnaghan equation of state fit curve.

$$h_m = h_c + h_s \tag{2}$$

Bao et al. [42] defined recovery resistance (R_s) as a material property to be an indicator of energy dissipation during an indentation cycle,

$$R_s = F_{max}/h^2 s, \tag{3}$$

Table 2
Elastic modulus and hardness determined from nano-indentation technique and bulk modulus and its derivate determined from high pressure expt are listed below. Bulk modulus obtained using third order Birch–Murnaghan equation of state for the alloys studied with first derivative of bulk modulus *K*' set as 4.

Sample/crystal structure	Elastic modulus *E* (GPa)	Hardness *H* (MPa)	Bulk modulus *K* (*K*' set as 4) (GPa)	Shear modulus *G* (GPa)	*K*/*G*	Poisson's ratio *v*
Ni_3Al	166.05 ± 5.08[A]	6.26 ± 0.28	186.3 ± 6.1[A]	61.95[A]	2.66	0.34[A]
Pm-3*m* ($L1_2$)	203.1 [19]		173.9 [22]	77.8[a]	2.24	0.31 [19]
			173 [23]			
			164.91 [24]			
			180 [25]			
			182 [26]			
			141.26 [27]			
Ni_3Al:B	161.00 ± 12.65	4.28 ± 0.27	201.8 ± 3.7[A]	58.88[A]	3.43	0.36[A]
Pm-3*m* ($L1_2$)						
Ni–Al–Cr	156.31 ± 9.23	4.37 ± 0.13	166.6 ± 5.8[A]	58.16	2.86	0.34
Pm-3*m* ($L1_2$) + *FCC*						

Prikhodko et al. [36].
Kayser [37].
Halevy [38].
Wu and Li [39].
Kim [40].
Zhang et al. [41].
[A] This study.

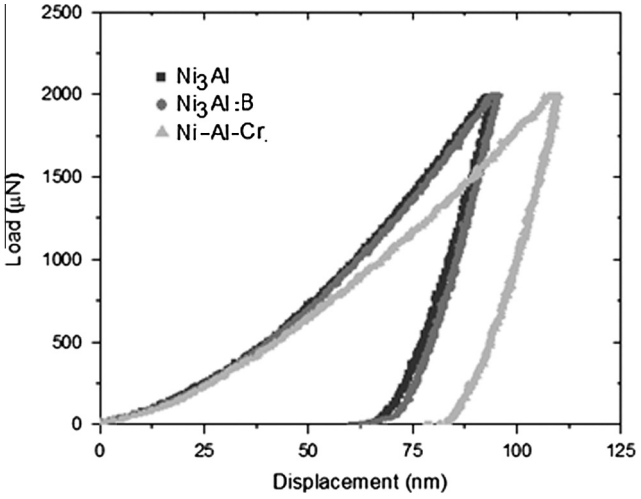

Fig. 6. Load–displacement curves for Ni_3Al, Ni_3Al:B and Ni–Al–Cr with the maximum load of 2000 μN.

and

$$R_s = 2.263\ E_r^2/H \tag{4}$$

where F_{max} is the peak load during nano-indentation, E_r and H are the reduced elastic modulus and the hardness in the nano-indentation. The values of *E* and *H* of the Ni alloys measured by nano-indentation technique are listed in Table 2. Bulk modulus is found to increase by 16 GPa for Ni_3Al:B while alloying with chromium decreases by 16 GPa. In the Ni–Al–Cr system, the compressive strength of both γ and γ′ phases remains indistinguishable within the experimental uncertainty. This indicates that the compressive strength of both the phases is influenced by the movement of defects and dislocations within the grains and through the grain boundaries thus keeping uniform compressibility in order–disorder systems. Our findings suggest that, under hydrostatic conditions, micro-alloying of Ni_3Al with boron increases the compressive strength by 8% while alloying with chromium shows a decrease of 10% when compared to the pure Ni_3Al alloy.

From the compressibility and the nano-indentation results, it can be noted that alloying with either 'B' or 'Cr' in Ni_3Al leads to a slight decrease in the elastic modulus and hardness with increase in the bulk modulus. Under the same load, the diamond indentor penetrated deeper in Ni–Al–Cr system than Ni_3Al and Ni_3Al:B, implying that Ni–Al–Cr was the least hard. The activation, mobility of dislocations is governed by the resolved shear modulus. In an attempt to correlate the hardness and elastic properties, we have calculated shear modulus from the experimental bulk modulus and elastic modulus using the relation for homogenous isotropic materials, given by.

$$v = (E/2G) - 1 \quad \text{and} \quad (3K - E)/6K \tag{5}$$

where '*K*' is the bulk modulus, '*E*' is the elastic modulus, '*G*' is shear modulus and '*v*' is Poisson's ratio. Shear modulus '*G*' is given by

$$G = 3KE/(9K - E) \tag{6}$$

Using the above relations, shear modulus and Poisson's ratios are determined for the three alloys and the results are listed in Table 2. Elastic modulus, shear modulus and hardness are highest for the Ni_3Al. Whereas, Ni_3Al:B shows highest bulk modulus. In Ni_3Al:B alloy, Boron segregation at the grain boundaries forms defects that causes an increase in bulk modulus by 8% higher than pure Ni_3Al. Whereas, addition of Cr to Ni_3Al shows opposite effect with a slight decrease in decrease in bulk modulus by 11% lower than the pure Ni_3Al. As per Pugh criterion, *K*/*G* value should be greater than 1.5 for ductile materials [43]. From Table 2, it can be noted that the Ni_3Al:B alloy has the highest *K*/*G* value indicating highest ductility and strength of all the alloys studied.

Nano-indentation results indicate a slight decrease of hardness and elastic modulus on alloying with boron or chromium. Hardness being a measure of plastic deformation, a decrease with alloying of B and Cr indicates decrease in the resistance to the plastic flow. On the other hand, elastic modulus caused by elastic deformation of crystal lattice is found to decrease on alloying with boron or chromium. Although *E*, *H*, *G* values decreases in both B and Cr alloyed systems, bulk modulus increases in the B-doped system relative to the pure Ni_3Al.

4. Conclusion

Presence of both γ and γ′ phases and the preferential segregation of Cr to the γ phase are confirmed by the HAADF-STEM image and EDS spectroscopy data. In the case of Ni_3Al alloyed with Cr, the decrease in compressibility can be attributed to the weakening of lattice due to the lattice site substitution of Cr. Whereas, in the case of B-doped Ni_3Al alloy, B segregates to the grain boundaries which hinders the movement of defects and dislocations between grains causing an increase in bulk modulus and a decrease in shear

modulus '*G*' relative to pure Ni_3Al. Ni_3Al:B has the highest K/G value which is indicative of highest strength and reveals it as a ductile material out of the Ni–Al alloys studied in the present work. Further, a slight increase in Poisson's ratio value for the B-doped alloy reflects this effect on the decrease in the compressive strength. For the Ni–Al–Cr system, the measured *E*, *G* and *B* decreases such that Poisson's ratio remains unchanged relative to pure Ni_3Al. Hence, we conclude that grain boundary strengtheners can improve the strength and ductility greater than the lattice site substituent.

Acknowledgements

The authors acknowledge support from the Air Force Office of Scientific Research (Grant No. FA9550-12-1-0456). The Advanced Light Source is supported by the Director, Office of Science, Office of Basic Energy Sciences, of the U.S. Department of Energy under Contract No. DE-AC02-05CH11231. Author SVR thanks Prof. Agarwal, Dept of Mechanical Engg. for useful discussions and help with nano-indentation measurements at the AMERI facility.

References

[1] R. Darolia, J. Metall. 43 (1991) 44–49.
[2] C.T. Liu, C.L. Fu, L.M. Pike, D.S. Easton, Acta Mater. 50 (2002) 3203–3210.
[3] N.S. Stoloff, C.T. Liu, S.C. Deevi, Intermetallics 8 (2000) 1313–1320.
[4] J.T. Guo, Order Intermetallic Compound NiAl, Science Press, Beijing, 2003.
[5] A. Chiba, S. Hanada, J. Mater. Sci. Technol. 9 (1993) 391–399.
[6] C. Barrett, T.B. Massalski, The Structure of Metals and Alloys, third ed., Structure of metals, New York, Pergamon, 1980. Chapter 10.
[7] S.W. Guan, W.W. Smeltzer, Oxid. Met. 42 (1994) 375–391.
[8] Nian Liu, Guo Dong Zhang, Lu Wu Jin, Fu Ju Zhang, Jian Qiang Zhang, Adv. Mater. Res. 1006 (2012) 581–582.
[9] Y. Wang, Z.-K. Liu, L.-Q. Chen, Acta Mater. 52 (2004) 2665–2671.
[10] C. Booth-Morrison, Z. Mao, R.D. Noebe, D.N. Seidman, Appl. Phys. Lett. 93 (2008) 033103.
[11] G.B. Viswanathan, J. Tiley, M. Chaudhari, A. Singh, P. Gopal, S. Nag, R. Banerjee, J. Du, Air force research lab wright-patterson Afb of materials and manufacturing directorate 7 (2011). AFRL-RX-WP-TP-2011-4218.
[12] M. Chaudhari, A. Singh, P. Gopal, S. Nag, G.B. Viswanathan, J. Tileyb, R. Banerjee, J. Du, Philos. Mag. Lett. 92 (2012) 495–506.
[13] P. Brož, M. Svoboda, J. Buršik, A. Kroupa, J. Havránková, Mater. Sci. Eng., A 325 (2002) 59–65.
[14] Aoki, Izumi, Nippon Kinzaku Gakkaishi 43 (1979) 1190.
[15] Yun Zhang, Dongliang Lin, Mater. Sci. Eng. A153 (1992) 354–369.
[16] E.P. George, C.T. Liu, D.P. Pope, Scripta Metall. Mater. 30 (1994) 37.
[17] D.A. Muller, S. Subramaniam, P.E. Batsob, J. Silox, S.L. Sass, Acta Mater. 44 (1996) 1637–1645.
[18] X.R. Qian, Y.T. Chou, J. Mater. Sci. 27 (1992) 1036–1044.
[19] Tresa M. Pollock, Sammy Tin, J. Propul. Power 22 (2006) 361–374.
[20] K.B. Pavorova, A.A. Drozd, N.K. Kazankskya, A.E. Morozov, A.V. Antovova, Russ. Metall. (2011) 209–220.
[21] Daniel C. Fredrickson, J. Am. Chem. Soc. 134 (2012) 5991–5999.
[22] Larry Jones, BES Interlaboratory study of Ni_3Al, Pittsburgh Airport Marriott Hotel (1987).
[23] G.K. Dey, Sadhana 28 (2003) 247–262.
[24] M. Hansen, Constitution of Binary Alloys, McGraw-Hill, New York, 1958.
[25] R. Ramesh, B. Pathiraj, B.H. Kolster, J. Mater. Sci. 29 (1994) 4764–4770.
[26] X. Sang, J.M. LeBeau, Ultramicroscopy 138 (2014) 28–35.
[27] Zhongwu Wang, CHESS High Pressure status update, News Magazine, 2009
[28] M. Kunz, A.A. MacDowell, W.A. Caldwell, D. Cambie, R.S. Celestre, E.E. Domning, R.M. Duarte, A.E. Gleason, J.M. Glossinger, N. Kelez, D.W. Plate, T. Yu, J.M. Zaug, H.A. Padmore, R. Jeanloz, A.P. Alivisatos, S.M. Clark, J. Synchrotron Radiat. 12 (2005) 650.
[29] Y. Chen, S.R. Bakshi, A. Agarwal, Surf. Coat. Technol. 204 (2010) 2709–2715.
[30] G.M. Pharr, W.C. Oliver, F.R. Brotzen, J. Mater. Res. 7 (1992) 613.
[31] W.C. Oliver, G.M. Pharr, J. Mater. Res. 7 (1992) 1564.
[32] Roger C. Reed, The Superalloys: Fundamentals and Applications, Cambridge University Press, Cambridge, 2006.
[33] J.C. Jamieson, J.N. Fritz, M.H. Manghnani, in: S. Akimoto, M.H. Manghnani (Eds.), High-Pressure Research in Geophysics, CAPJ, Tokyo, 1982, pp. 27–48.
[34] F. Birch, Phys. Rev. 71 (1947) 809.
[35] F.D. Murnaghan, Proc. Nat. Acad. Sci. 30 (1944) 244.
[36] S.V. Prikhodko, J.D. Carnes, D.G. Isaak, H. Yang, A.J. Ardell, Metall. Mater. Trans. A. 30A (1999) 2403.
[37] F.X. Kayser, C. Stassis, Phys. Status Solidi (A) 64 (1981) 335.
[38] I. Halevy, S. Salhov, A. Broide, O. Yeheskel, I. Yaar, Joint 2oth AIRAPT – 43rd EHRPG Int. Conf. on High Press. Sci. and Technol., Karlsruhe (2005) 36.
[39] Q. Wu, S. Li, Comput. Mater. Sci. 53 (2012).
[40] D.E. Kim, Intermetallics 18 (2010).
[41] J.-H. Zhang, S.-Q. Wu, Y.-H. Wen, Z.-Z. Zhu, J. Atmos. Mol. Sci. 1 (2010) 253.
[42] Y.W. Bao, W. Wang, Y.C. Zhou, Acta Mater. 52 (2004) 5397.
[43] S.F. Pugh, Philos. Magn. 45 (1954) 823.